polymers

MDPI

*Article*

# CuNi Alloy NPs Anchored on Electrospun PVDF-HFP NFs Catalyst for $H_2$ Production from Sodium Borohydride

**Ahmed Abutaleb**

Department of Chemical Engineering, College of Engineering, Jazan University, Jazan 11451, Saudi Arabia; azabutaleb@jazanu.edu.sa

**Abstract:** Non-noble $Cu_xNi_{1-x}$ (x = 0, 0.1, 0,2, 0.3, 0.4, 0.5, 0.6, 0.7, 0.8, 0.9, 1) alloy nanoparticles supported on poly(vinylidene fluoride-co-hexafluoropropene) (PVDF-HFP) nanofibers (NFs) are successfully fabricated. The fabrication process is executed through an electrospinning technique and in situ reduction in $Cu^{2+}$ and $Ni^{2+}$ salts. The as-synthesized catalysts are characterized using standard physiochemical techniques. They demonstrate the formation of bimetallic NiCu alloy supported on PVDF-HFP. The introduced bimetals show better catalytic activity for sodium borohydride (SBH) hydrolysis to produce $H_2$, as compared to monometallic counterparts. The $Cu_{0.7}$ $Ni_{0.3}$/PVDF-HFP catalyst possesses the best catalytic performance in SBH hydrolysis as compared to the others bimetallic formulations. The kinetics studies indicate that the reaction is zero order and first order with respect to SBH concentration and catalyst amount, respectively. Furthermore, low activation energy (Ea = 27.81 kJ/mol) for the hydrolysis process of SBH solution is obtained. The excellent catalytic activity is regarded as the synergistic effects between Ni and Cu resulting from geometric effects over electronic effects and uniform distribution of bimetallic NPs. Furthermore, the catalyst displays a satisfying stability for five cycles for SBH hydrolysis. The activity has retained 93% from the initial activity. The introduced catalyst has broad prospects for commercial applications because of easy fabrication and lability.

**Keywords:** chemical reaction engineering; nanofibers; electrospinning; sodium borohydride; hydrogen generation

check for updates

**Citation:** Abutaleb, A. CuNi Alloy NPs Anchored on Electrospun PVDF-HFP NFs Catalyst for $H_2$ Production from Sodium Borohydride. *Polymers* **2023**, *15*, 474. https://doi.org/10.3390/polym15030474

Academic Editor: Davood Kharaghani

Received: 17 December 2022
Revised: 1 January 2023
Accepted: 6 January 2023
Published: 17 January 2023

**Copyright:** © 2023 by the author. Licensee MDPI, Basel, Switzerland. This article is an open access article distributed under the terms and conditions of the Creative Commons Attribution (CC BY) license (https://creativecommons.org/licenses/by/4.0/).

## 1. Introduction

The fast growth in the world population is leading to an increase in global energy consumption that is primarily formed from fossil fuels (e.g., petroleum oil, coal, and natural gas). Combustion of fossil fuels produces toxic gases (e.g., carbon dioxide, nitrous oxide, etc.) that deteriorate the ecological environment [1–3]. Thus, the search for alternative and sustainable energy has become urgent worldwide. Hydrogen ($H_2$) is considered one of the most hopeful energy carrier sources because of its high energy content and eco-friendly characteristics such as zero-pollutant emissions [4]. However, the practical application of $H_2$ in large quantities (e.g., fuel cell vehicles) suffers from unsafe and inefficient $H_2$ storage methods (e.g., compressed gasses or cryogenic liquids) at mild conditions, which is attributed to the low $H_2$ density > 5 wt% [5–9]. In recent years, metal hydrides (e.g., sodium borohydride ($NaBH_4$, SBH), lithium hydride (LiH), sodium aluminum hydride ($LiAlH_4$), lithium aluminum hydride ($LiAlH_4$), and lithium borohydride ($LiBH_4$)) have been recognized as promising hydrogen reservoirs because of their extraordinary $H_2$ storage density [10–12]. Amongst them, SBH is considered one of the ideal candidates for an $H_2$ reservoir owing to its low density and low molecular weight, low cost, non-toxicity, and high hydrogen content (~10.8 wt.%). $H_2$ can be generated through hydrolysis of SBH in the presence of appropriate catalysts like noble (e.g., Pt, Ru, and Pd) and non-noble metallic (e.g., Ni, Co, and Cu) nanoparticles (NPs) and their alloys [13–15]. Recently, bimetallic Cu-M (M=Fe, Co, Ni) with different geometries and compositions has become very attractive

in the fast production of $H_2$ from hydrogen storage materials [16–19]. However, NPs suffer from high agglomeration during $H_2$ release as a vigorous hydrolysis reaction occurs and converts the NPs into regular particles [8,20–22]. To avoid the agglomeration issue, NPs were supported on different matrices such as carbon, silica, $TiO_2$, zeolite, $Al_2O_3$, and others [23–26]. Ayman Yousef et al. [27] prepared NiCu nanorods@carbon NFs and found the superior catalytic activity for AB hydrolysis. Jun Zhang et al. [28] demonstrated porous hierarchical Cu@Ni cubic cage as a very active catalyst for AB hydrolysis. However, the catalysts in the powder form suffer from some issues such as (1) the separation of the suspension-powder NPs from the solution is difficult, (2) the NPs tend to coalesce and agglomerate, and (3) the suspension-powder NPs are difficult to apply on continuous flow. R. Fernandes et al. [29] supported NPs over thin films to avoid these issues. However, the fixation of NPs on the thin film decreased the NPs' exposed surface [7]. Polymer NFs have been introduced as catalytic supports for numerous metallic and non-metallic NPs [30–35] and used in different chemical reactions [36–38]. Catalysts made with polymer NF supports are very easy to recycle and reuse efficiently. Additionally, NFs are well-known to have huge surface areas; most NFs possess double the surface area of continuous thin films [39]. Kim and his coworkers have prepared hybrid NFs composed from polyvinylidene fluoride (PVDF) and $CoCl_2$ for $H_2$ production from SBH [40–45]. In another work, they have prepared a PVDF/$CoCl_2$/Y-Zeolite effective catalyst to generate $H_2$ from SBH hydrolysis. The fabricated catalysts showed outstanding performance with fair chemical stability and reusability. The presence of regular and interconnected pores provides easy access for reactants and the release of products, evolved $H_2$. It is well-known that fabricated NFs via a simple electrospinning technique can produce a highly uniform and interconnected pores structure within a large surface-to-volume ratio [20,46–51]. In recent years, electrospun nanofibrous PVDF-HFP mats have been fabricated and applied in different important applications such as a water treatment, polymer electrolyte, and catalytic support for different reactions [52–56]. PVDF-HFP is one of the most appropriate host polymers for making hybrid composites as compared to various host polymers. PVDF-HFP has excellent electrochemical and chemical stability with great affinity to absorb electrolyte solution. The attachment of metal NPs on the surface of PVDF-HFP NFs has dual effects, namely that it [57] (1) decreases the polymer crystallinity and (2) enhances the electrolyte solution uptake, which lead to an improvement in the SBH and catalyst surface contact. Accordingly, PVDF-HFP is an excellent catalytic support candidate to support metallic and non-metallic NPs.

This study aims to prepare $Ni_xCu_{1-x}$ NPs-PVDF-HFP NFs as a bimetallic catalyst for $H_2$ production from SBH hydrolysis. The fabricated NFs were prepared using an electrospinning technique followed by a chemical reduction process. Characterizations of the fabricated electrospun catalysts proved the fabrication of $Ni_xCu_{1-x}$ bimetallic nanoalloy supported on PVDF-HFP NFs. The introduced NFs demonstrated excellent catalytic activity toward $H_2$ generation from SBH. The fabricated $Ni_{0.7}Cu_{0.3}$/PVDF-HFP NFs exhibited the maximum catalytic activity. Furthermore, this composition showed good stability six times.

## 2. Materials and Methods

### *2.1. Materials*

Poly(vinylidene fluoride-co-hexafluoropropene) ((PVDF-HFP), 98% assay, (MW = 65,000 g/mol)), nickel (II) acetate tetrahydrate ((NiAc), 98% assay), copper (II) acetate mono-hydrate ((CuAc), 98% assay), and sodium borohydride (SBH, NaBH4, 98% assay) were purchased from Aldrich Co., St. Louis, MO, USA. N, N-dimethylformamide (DMF, reagent grade, 99% assay), and acetone were brought from Fluka, Al-Khobar 31952 Saudi Arabia. All chemicals were utilized without any further modifications.

### *2.2. Experimental Work*

All different proposed catalysts were fabricated through three consequence major steps: (i) preparation of electrospinning solutions, (ii) fabrication of polymeric NFs using

electrospinning technique, and finally (iii) reduction in the catalytic acetate precursor into their metallic forms.

To prepare the electrospinning solutions, first, polymer solutions, 15 wt.% PVDF-HFP, were prepared by dissolving 1.5 g of PVDF-HFP powder in a solvent mixture of DMF and acetone (4:1). The polymeric solutions were mixed in a magnetic stirrer for at least 6 h to make very homogenous sol–gel solutions. Second, different composition from the catalytic precursors, NiAc and CuAc, were added to 20 g of the prepared homogenous PVDF-HFP solutions, separately. The amount of NiAc and CuAc were adjusted to fabricate NFs with $Ni_{1-x}Cu_x$ (x = 0–0.9). To ensure perfect dispersion of the catalytic precursors, the electrospinning sol–gel solutions were stirred, after adding the catalytic precursors, for 5 h at 50 °C. The NiAc-CuAc/PVDF-HFP solutions were finally cooled at room temperature to become ready to be electrospun.

The prepared electrospinning solutions were then electrospun using a lab-scale electrospinner to fabricate polymeric NFs with different catalytic precursors compositions. The electrospinning set-up consists of three major components: solution reservoir to hold the electrospinning solution, power supply to generate an electrical field, and a collector to collect the fabricated NFs. The fabricated polymeric solutions were placed in a reservoir, a 5 mL plastic syringe. The electrical field was generated by inserting a copper wire inside the plastic syringe from one end (positive electrode) while the other side, the collector, was grounded. The rotating drum collector was covered with aluminum foil to collect the fabricated NFs. The electrospinning operating conditions were fixed at room temperature and pressure, 20 kV and 18 cm distance between the syringe and the collector. Generally, most of the solvents evaporate while the NFs travel from the syringe to the collector; however, some residual solvent stays in the fabricated NFs. Hence, the fabricated NF mats were dried at 40 °C under vacuum overnight to ensure full evaporation of the solvent mixture.

### *2.3. Chemical Reduction in CuAc and NiAc Supported on PVDF-HFP NFs*

To reduce catalytic precursors and convert NiAc and CuAc into their pure metallic forms, SBH was used as a reducing agent. Typically, to start the reduction process, first, 100 mL of methanol was placed in a 500 mL beaker. Then, the fabricated electrospun nanofibrous mats were immersed in the methanol solution. After that, SBH was added in the beaker and stirred at 1000 rpm. The molar ratios between metals precursor and SBH were adjusted at 1:5 to obtain a complete reduction reaction. To prevent vigorous reduction reactions, the reduction reaction was operated at low temperature. It was noticed that as soon as the fibrous mat was immersed in the solution, a gas bubble ($H_2$) was produced with a green-to-black color change, indicating that NiAc and CuAc converted into Ni and Cu metals, respectively. The fibrous mat was kept in the SBH solution until no $H_2$ bubbles were seen. The produced mat was washed by ethanol and DI water to eliminate impurities. Last, the reduced nanofibrous mat was dried overnight at 40 °C under vacuum.

Equation (1) shows that the methanolysis reaction produces a by-product, sodium tetra methoxy borate ($NaB(OCH_3)_4$) [8]. This by-product reacts with water during the washing process, as shown in Equation (2), and produces methanol and sodium borate, $NaBO_2$, both of which are washed away with the excess water.

$$\mathbf{NaBH_4 + 4CH_3OH \rightarrow NaB(OCH_3)_4 + 4H_2} \quad (1)$$

$$\mathbf{NaB(OCH_3)_4 + 2H_2O \rightarrow NaBO_2 + 4CH_3OH} \quad (2)$$

It is worth mentioning that researchers usually use aqueous SBH to reduce metal salts [39]. However, SBH here was dissolved in methanol and used to execute the reduction step. In fact, aqueous SBH was initially applied as a reducing agent, and it was seen that the reduction reaction was much slower than the SBH/methanol reducing agent.

Using methanol instead of water provides important advantages. For example, the by-product, $NaB(OCH_3)_4$, does not rapidly polymerize into various types of polyborates. Preventing the precipitation of $NaB(OH)_4$ is necessary to stop the poisoning of the cata-

lyst [58,59]. Hongming et al. [60] used hydrothermal and reduction procedures to prepare ultrafine Co NPs@carbon nanospheres as an effective catalyst for the generation of $H_2$ from SBH hydrolysis. Due to the insolubility of $NaBO_2$ in ethanol, partial $NaBO_2$ was precipitated out together with the Co NPs in the water media. This could separate the Co nanoparticles and further prevent them from agglomerating into larger clusters. They found that the reduction in Co ions in the ethanol solution media was more effective than in the water media. In the end, the $NaBO_2$ was removed by washing it with DI water. The surfaces of the membranes that were electrospun using $Ni^{2+}$ $Cu^{2+}$/PVDF-HFP were green in hue. The chemical reduction in these metallic ions has a tendency to modify the color of their linked polymeric membranes into a black-look-alike black-dyed piece of fabric. This change in color is what indicated the formation of ultrasmall NiCu NPs on the surface of PVDF-HFP membranes.

### 2.4. Characterization

The fabricated catalytic NFs morphology was characterized by a scanning electron microscope (SEM, Hitachi S-7400, Japan) equipped with an energy-dispersive X-ray (EDX). A Fourier transform infrared (FTIR), using the smart ATR-FTIR model "Nicolet iS 10" (Thermo Fisher Scientific, Waltham, MA, USA) equipped with the specular reflectance, was also used to study the interaction between Ni Cu NPs and PVDF-HFP NFs. The fabricated NFs were positioned at the top of the spectrophotometer and the scanning range was 400–3500 $cm^{-1}$. X-ray diffraction (Rigaku Co., Tokyo, Japan) with Cu Kα (λ = 1.54056 Å) was utilized to determine the catalysts' crystalline structure and crystal size. An X-ray photoelectron spectroscopy analysis (XPS, AXIS-NOVA, Kratos Analytical, Manchester, UK) was conducted with the following conditions: base pressure of $6.5 \times 10^{-9}$ Torr, resolution (pass energy) of 20 eV, and scan step of 0.05 eV/step.

### 2.5. SHB Catalytic Hydrolysis Reaction

To run the reaction experiments, a two-neck flask was used as a reactor. The reactor was placed on a magnetic stirrer. The magnetic stirrer provided both mixing and heating. The reaction temperature was measured by a thermometer. The flask was connected by a plastic tube to a gradually cylinder filled with water to measure the generated $H_2$ gas. Water displacement from the gradually cylinder was reflected in the volume of $H_2$ generation gas. To start the reaction, first, 100 mg of the prepared catalytic membranes was placed inside the flask. Then, 50 mL of 1 mmol of SBH was fed to the reactor and mixed at 100 rpm and the temperature was kept at 25 °C.

The catalytic hydrolysis reaction was started rapidly without induction time when catalytic NFs were conducted in the reactor. The kinetics of the hydrolysis reaction was studied by changing the amount of the catalysts, concentration of SBH, and temperature. To study the effect of a catalyst on the $H_2$ production, different amounts of catalysts (100, 150, 200, and 250 mg) have been used. The effect of SBH concentration (1, 2, 3, and 4 mmol) on $H_2$ production was also studied. To calculate the reaction activation energy, different reaction temperatures (298, 308, 318, and 328 K) have been studied. The durability of the introduced NFs was also studied through a recycling process. The reusability test has been conducted at 100 mg, 1 mmol, and 298 K of catalyst, SBH, and temperature, respectively. The catalyst has been used at all cycles without any washing. At each cycle, 1 mmol SBH was added and other parameters were kept constant.

## 3. Results and Discussion

Increased interconnections, flexibility, excellent porosity, and remarkable surface-to-volume ratios are just a few of the potential benefits of a polymeric nanofibrous membrane produced using the electrospinning approach [61,62]. The semi-crystalline nature, high thermal stability, improved dielectric constant, hydrophobicity, and piezo- and pyroelectric properties of PVDF-HFP make it one of the most suitable polymeric materials for producing these films [63,64]. SEM images of dried electrospun PVDF-HFP nanofibrous mats, at both

low and high magnifications, proved the fabrication of an excellent nanofibrous structure devoid of beads (Figure 1A,B). It is well-known that the electrospinning technique produced nanoporous-structured NFs. These nanopores are generated in the electrospun NFs because of the high evaporation rate of solvents, especially acetone. Solvent evaporation happens when the NFs travel from the positive-charge electrode, syringe needle, to the negative electrode, rotating drum. This nanoporous structure is ideal for the nucleation of Ni and Cu crystals. In addition, since the CuAc and NiAc precursor salts have high water content, the produced hydrophobic PVDF-HFP membranes exhibit an increased demixing rate within the liquid–liquid phases. This demixing results in the formation of a high number of pores on their structure [65]. As a result, the analyte molecules would be able to get trapped in the pores with the minimal possibility of diffusion resistance, so making $H_2$ evolution more straightforward. High electrical conductivity and gelation of the PVDF-HFP solution, together with the formation of maximal elongation of a jet along its axis, are two additional benefits of the presence of metal salts in the process of producing nanoscale polymeric NFs [44].

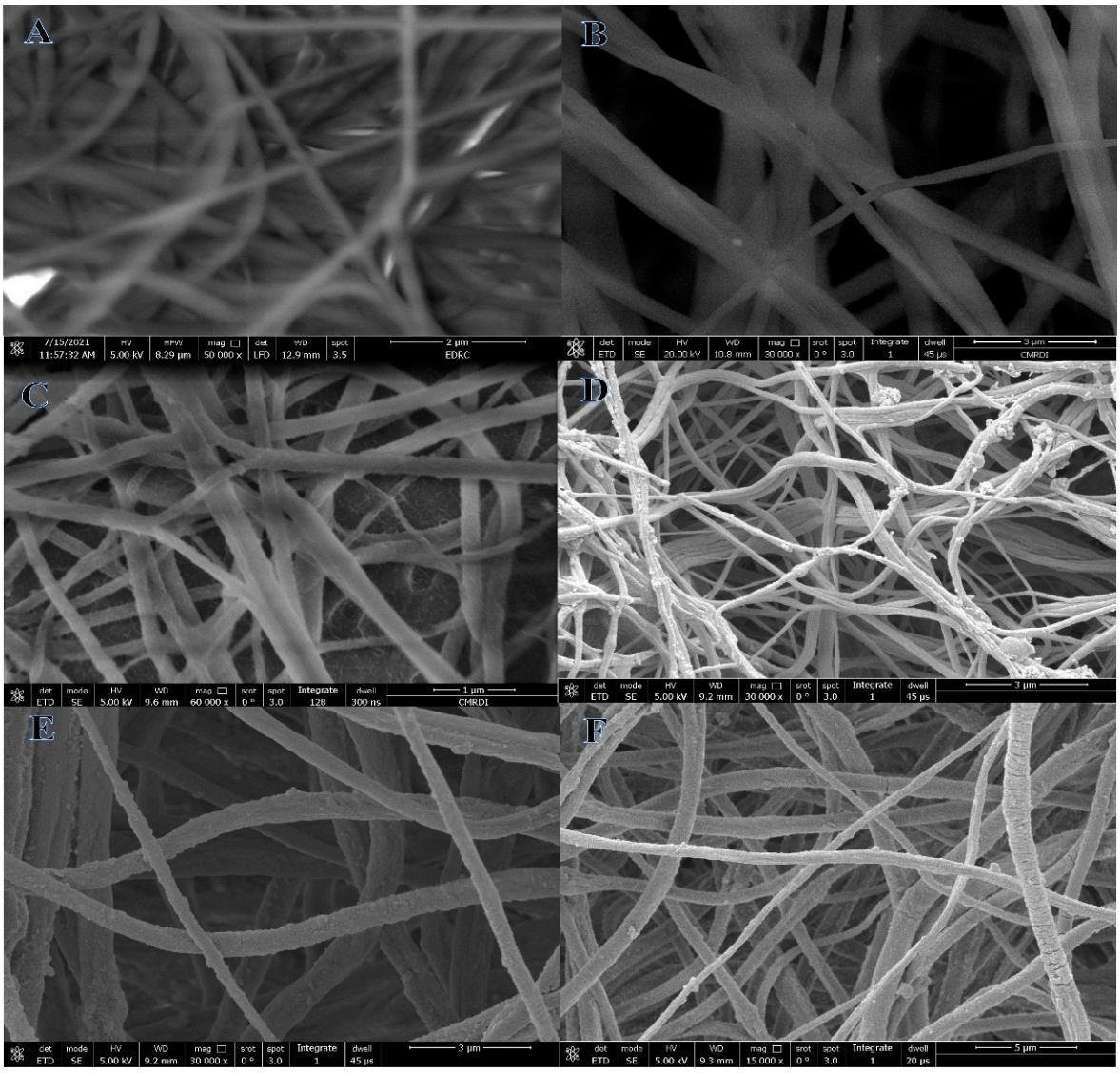


**Figure 1.** Low and high magnifications of SEM images PVDF-HFP (**A**), $Ni_{0.9}Cu_{0.1}$/PVDF-HFP (**B**), $Ni_{0.7}$ $Cu_{0.3}$/PVDF-HFP (**C**), $Ni_{0.5}Cu_{0.5}$/PVDF-HFP (**D**), $Ni_{0.3}Cu_{0.7}$/PVDF-HFP (**E**), $Ni_{0.1}Cu_{0.9}$/PVDF-HFP NF membranes (**F**).

Figure 1C–F show SEM images of electrospun $Ni_{0.3}Cu_{0.7}$-PVDF-HFP and $Ni_{0.1}Cu_{0.9}$-PVDF-HFP NFs, respectively. Rough and bead-free NFs are created, as seen in the figure. In addition, the nanoporous nature of PVDF-HFP NFs means that reduced Ni and Cu ions may cover their surface after the mats are formed.

On display in Figure 2A–D is an elemental mapping image of the $Ni_{0.7}Cu_{0.3}$/PVDF-HFP membrane NFs. It is clear that there is a large distribution of Ni and Cu NPs throughout the membrane NFs, and this is supported by the pictures obtained from the SEM. The figure displays the EDX curve for the $Ni_{0.3}Cu_{0.7}$-PVDF-HFP membrane NFs (Figure 3A,B). The detected chemical composition of the product are the elements carbon, copper, nickel, and fluorine. The weight % of Ni and Cu that are developed at different points is shown in the inset of Figure 3B. It is obvious that NPs are distributed greatly throughout the NFs, and their composition is perfectly similar to that of the precursors from which they were originated.

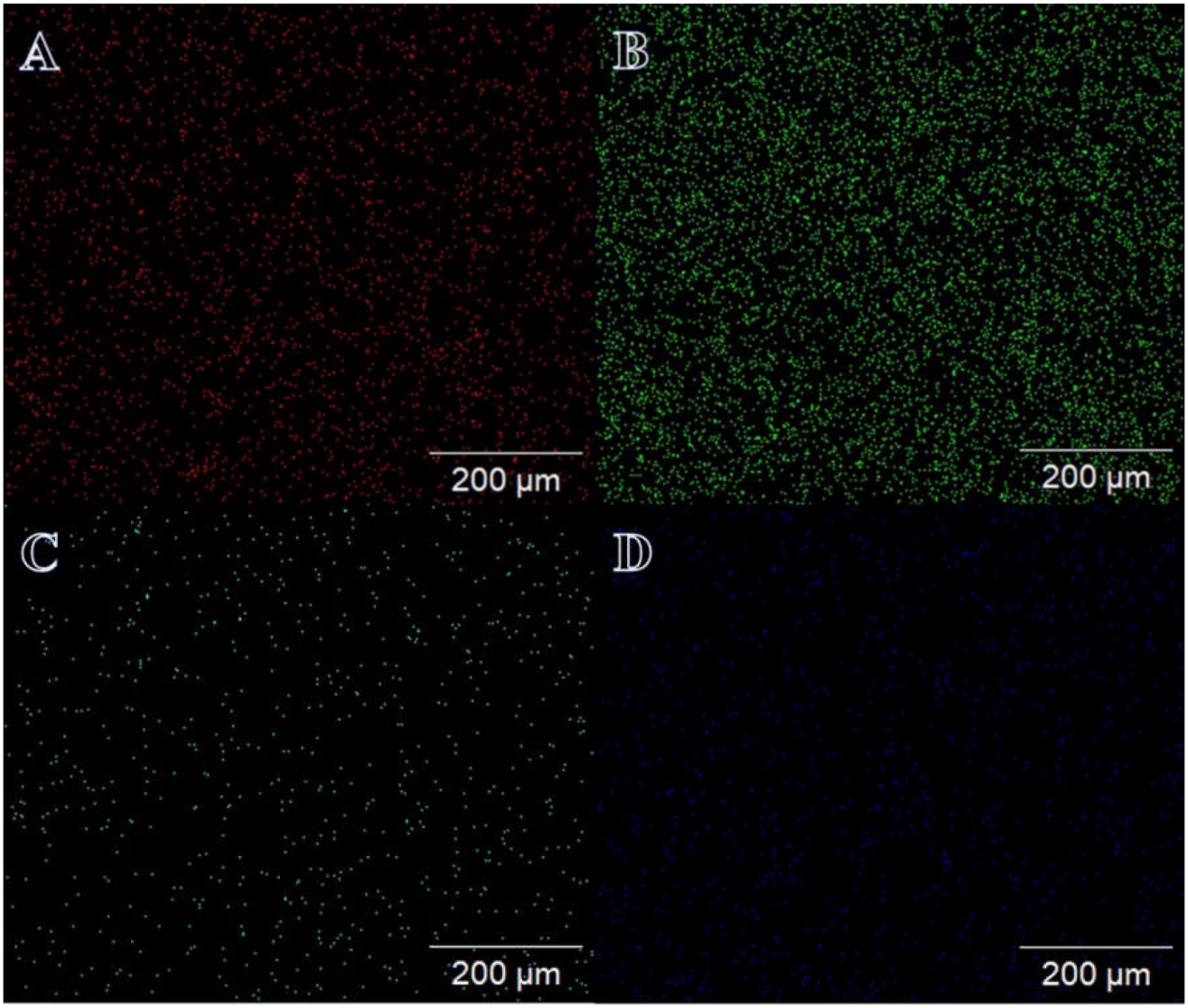


**Figure 2.** Elemental mapping to show the distribution of fluorine (**A**), carbon (**B**), nickel (**C**), and copper (**D**) in the $Ni_{0.3}Cu_{0.7}$/PVDF-HFP NF membrane.

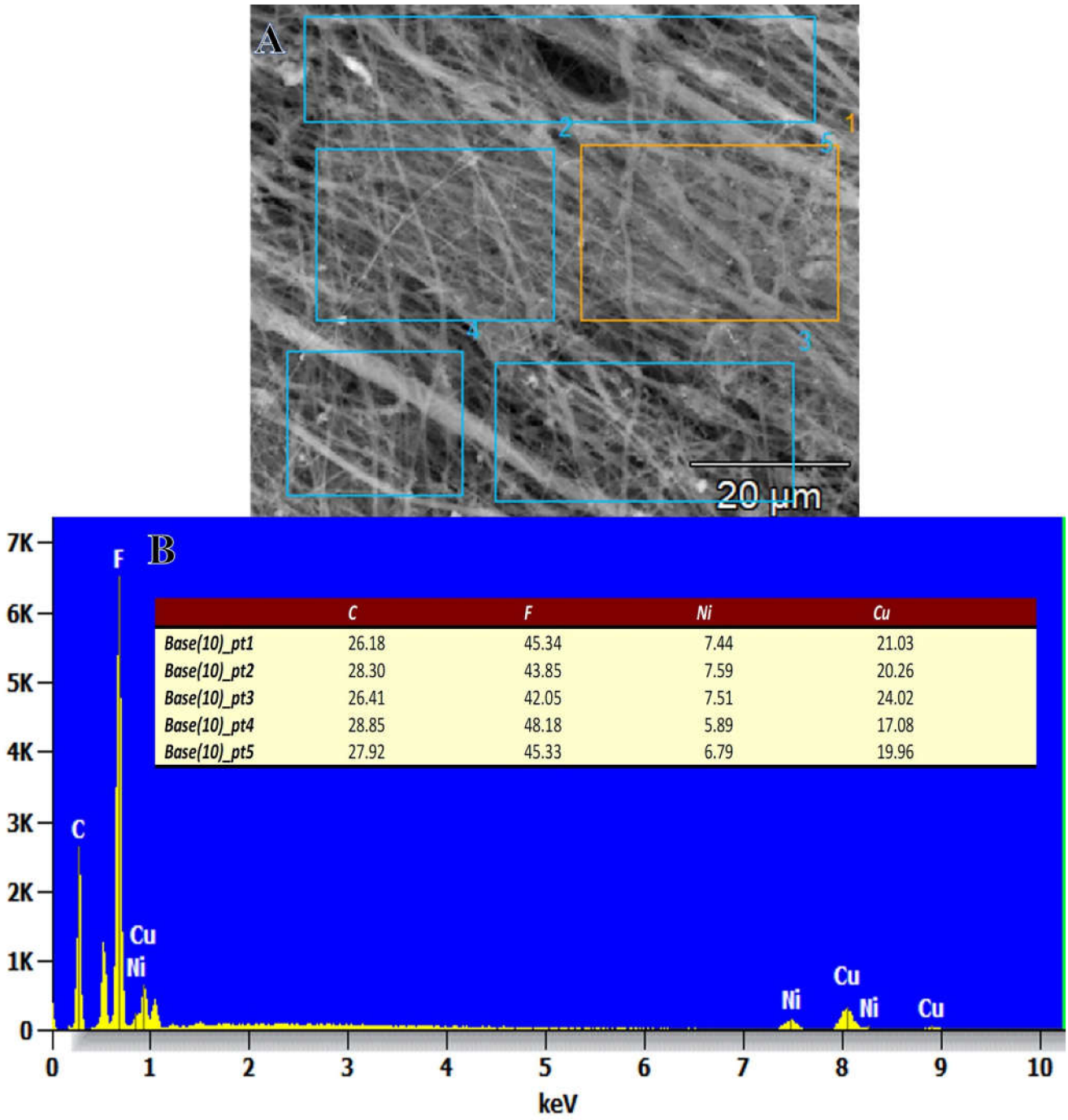


**Figure 3.** (**A**) SEM image and (**B**) EDX chart of $Ni_{0.3}Cu_{0.7}$/PVDF-HFP NF membrane at different SEM image points.

Figure 4 shows the XRD diffraction patterns of the fabricated electrospun membranes. The $Ni_{0.3}Cu_{0.7}$/PVDF-HFP NFs, in its as-spun state, displayed characteristic diffraction peaks at 2 $\theta$ of 18.2°, 20°, 26.6°, and 36.15°, which correspond to the characteristic reflection planes of (100), (020), (110), and (021) [52,66]. The NiCu/PVDF-HFP catalyst had additional diffraction peaks at 43.4° and 50.4°, which are attributed to the (111) and (200) reflection planes, respectively. These planes are congruent with those of Ni (JCPDS 04-0850) and Cu (JCPDS, File no. 04-0836) as a result of their crystal structures being identical (face-centered cubic), of the very close crystal lattice parameters between Cu (3.615 Å) and Ni (3.523 Å), and of the same space group of Fm3m, which can be formed as a solid solution.

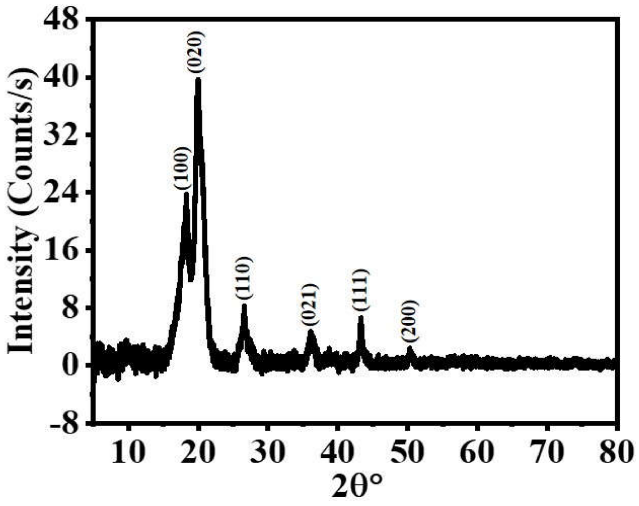


**Figure 4.** XRD results of $Ni_{0.3}Cu_{0.7}$/PVDF-HFP NF membranes.

Using SBH as an effective reducing agent in a $CH_3OH$ medium, metallic Ni and Cu NPs were produced on the PVDF-HFP NFs surface. Because of their disparate reduction potentials ($E_0$ $Cu^{++}/Cu^0$ = +0.34 V vs. SHE and $E_0$ $Ni^{++}/Ni^0$ = −0.25 V versus SHE), SBH is more suited to reducing Cu ions to $Cu^0$ than Ni ions to $Ni^0$. First, the generation of $Cu^0$ NPs stimulated SBH hydrolysis. Then, the production of an active intermediate, Cu-H species, becomes the key to facilitate $Ni^{++}$ reduction. As a result, $Cu^0$ plays a substantial role in improving the formation of the desired catalytic structure.

The FTIR spectra of PVDF-HFP and NiCu/PVDF-HFP fibrous mats are shown and explained in Figure 5. It is obvious that both fibrous mats had recognizable vibrational bands that were similar to one another. The phases of α and β were identified thanks to the corresponding peaks that occurred at frequency values of 749 and 837 $cm^{-1}$ [67]. Two other important vibrational bands, centered at 672 and 872 $cm^{-1}$, were designated for the CF and $CH_2$ wagging of vinylidene units in the amorphous phase of the PVDF-HFP film. These bands were found in the amorphous phase of the film. Additionally, the symmetric C-F stretching, the $CF_2$ stretching, and the deformed vibrations in this fibrous mat were also revealed via their respective bands at 1071, 1175, and 1400 $cm^{-1}$ [68]. During the process of fabricating the polymeric membrane, the addition of nickel and copper precursor salts caused the appearance of two more peaks. The stretching vibration maxima at 1561 $cm^{-1}$ proved the production of NiO and CuO species inside this nanomaterial [69].

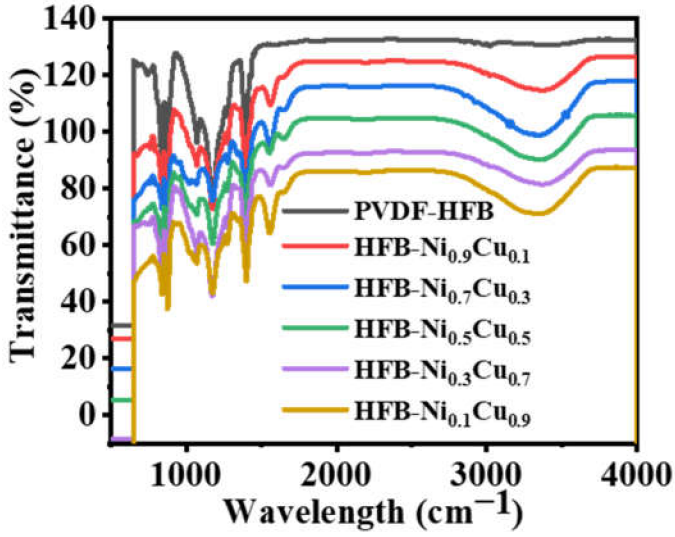


**Figure 5.** FTIR charts of PVDF-HFP and $Ni_xCu_{1-x}$/PVDF-HFP NF membranes.

*Hydrogen Release from SBH*

In a two-neck flask connected to a graduated burette containing water, the catalytic activity of the fabricated catalysts (Ni/PVDF-HFP and $Ni_xCu_{1-x}$/PVDF-HFP) toward $H_2$ production from SBH was determined. Figure 6 shows the catalytic activity of various $Ni_xCu_{1-x}$/PVDF-HFP formulations compared to that of the mono-metallic Ni/PVDF-HFP; the bimetallic alloys display a high hydrogen-production volume. The $H_2$ production rate initially grew and subsequently fell over the course of a given time period. The catalytic reaction in this case seems to take place on the metal catalyst's surface [19]. These findings provide strong evidence for a significant role for the synergistic interaction between Cu and Ni in the hydrolysis of SBH. The synergistic effects of NPs alloy can be attributed mostly to the electronic effects, which become significant when the metal atoms have considerable variances in electronegativity and geometric effects [20]. The electronegativities of Cu and Ni are so similar: 1.90 and 1.91, respectively; therefore, it is likely that the obtained synergetic effects of the fabricated $Ni_xCu_{1-x}$/PVDF-HFP catalysts are mostly attributable to the geometric effects rather than the electronic effects. Since both Cu and Ni have an A1-type crystal structure, the formation of CuNi alloy NPs allows Ni to replace part of the Cu in the Cu lattice while still allowing the Cu crystal system to maintain its A1-type crystal structure, resulting in strong synergistic effects between Cu and Ni. The bimetallic catalyst $Ni_{0.3}Cu_{0.7}$ showed the maximum catalytic activity, releasing 96 mL of $H_2$ in 36 min. The other four bimetal catalysts ($Ni_{0.9}Cu_{0.1}$, $Ni_{0.7}Cu_{0.3}$, $Ni_{0.5}Cu_{0.5}$, and $Ni_{0.1}Cu_{0.9}$) catalyzed $H_2$ release equivalents of 71, 79, 87, and 83 mL, respectively, in the same time period. In terms of catalytic activity, the order of the engaged bimetal catalysts is as follows: $Ni_{0.3}Cu_{0.7}$ > $Ni_{0.5}Cu_{0.5}$ > $Ni_{0.1}Cu_{0.9}$ > $Ni_{0.7}Cu_{0.3}$ > $Ni_{0.9}Cu_{0.1}$. According to the findings, the NiCu's catalytic activity changes when the Cu/Ni ratio is altered. When comparing the catalytic activity of all five bimetal catalysts, it is found that as the percentage of Cu increases, the catalysts become more effective. It is theorized that an increase in the Cu content of NiCu alloy facilitates the passage of more electric charge from Cu to Ni, resulting in the generation of more active sites on the catalytic surface. The greater catalytic activity of bimetallic alloy in comparison to mono metals have been observed in other metal catalysts [21–26]. For example, Li [27] and Yamada [28] have independently discovered that the Cu concentration of a Cu-based bimetal catalyst considerably influences its catalytic activity. Furthermore, the low catalytic activity and nearly nonexistent catalytic activity of pure PVDF-HFP toward hydrolysis of SBH are readily apparent. These findings give conclusive evidence that the bi-functional impacts of CuNi-alloy NPs and PVDF-HFP considerably improved the reaction activity of the $Ni_{0.3}Cu_{0.7}$/PVDF-HFP catalyst, where the catalytic support PVDF-HFP NFs may serve as a suitable matrix for CuNi NPs despite their lack of involvement in SBH hydrolysis. The mechanism involved two main steps: at first, SBH is adsorbed on the CuNi nanoparticles' surface to produce the activated intermediate metal-H, a condition precedent to the hydrolysis process. Then, when water was thrown at the metal-H species, $H_2$ was generated [29,30].

The performance of the fabricated nanofibrous catalysis is a function of several factors including SBH concentration, reaction temperature, catalyst amount, and catalyst reusability. Therefore, the effect of operating conditions on the performance of the best fabricated catalyst, $Ni_{0.3}Cu_{0.7}$/PVDF-HFP, was studied. First, the effect of the amount of the catalyst on $H_2$ generation, at 25 °C and 1 mmol of SBH, was studied. Increases in the catalyst amount, as shown in Figure 7a, resulted in an increase in the generated $H_2$ volume. In fact, increasing the catalyst dose from 100 mg to 250 mg shortened the time it took for $H_2$ evolution from 36 minutes to 12 minutes. So, for all reactions carried out under similar conditions, the time required to produce $H_2$ reduces practically linearly as the amount of catalyst used increases. While this relationship is only somewhat linear, it does show that the hydrolysis process is first-order with regard to the amount of catalyst within a slope of 1.1 (Figure 7b). As a result, 100 mg of $Ni_{0.3}Cu_{0.7}$/PVDF-HFP was selected for use in the following studies.

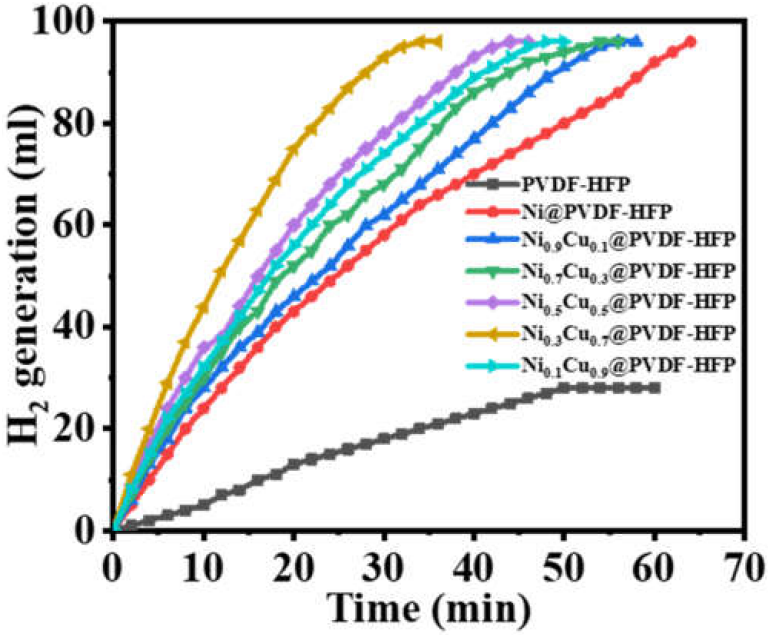


**Figure 6.** Influence of $Ni_xCu_{1-x}$/PVDF-HFP NF membranes on $H_2$ production from SBH hydrolysis at 100 mg catalyst, 1 mmol [SBH], and 298 K.

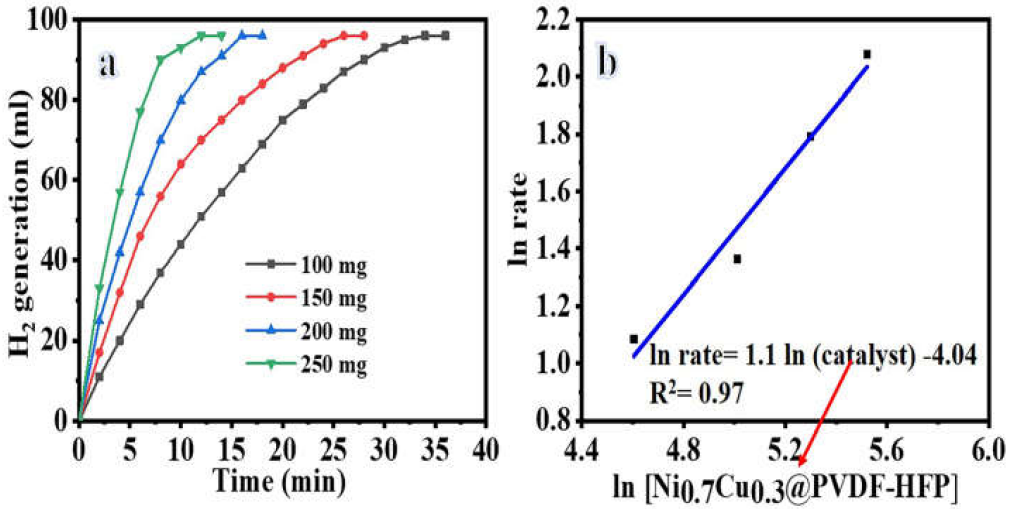


**Figure 7.** The effect of changing the amount of $Ni_{0.3}Cu_{0.7}$/PVDF-HFP NFs on $H_2$ production (**a**), and the $H_2$ production rate logarithmic value vs. at catalyst amount logarithmic value (**b**) at 1 mmol [SBH] and 298 K.

Figure 8a shows the results of an experiment that investigated the impact of SBH concentration on reaction rate using 100 mg of $Ni_{0.3}Cu_{0.7}$/PVDF-HFP catalyst and a temperature of 25 °C. The rate of produced $H_2$ at the outset increases linearly with the concentration of SBH, as shown in the figure. This demonstrates that the volume of $H_2$ generation does not rely on the amount of SBH present. Since the start, SBH concentration has no effect on the hydrolysis process, and the slope of 0.06 indicates that the hydrolysis reaction is in zero order.

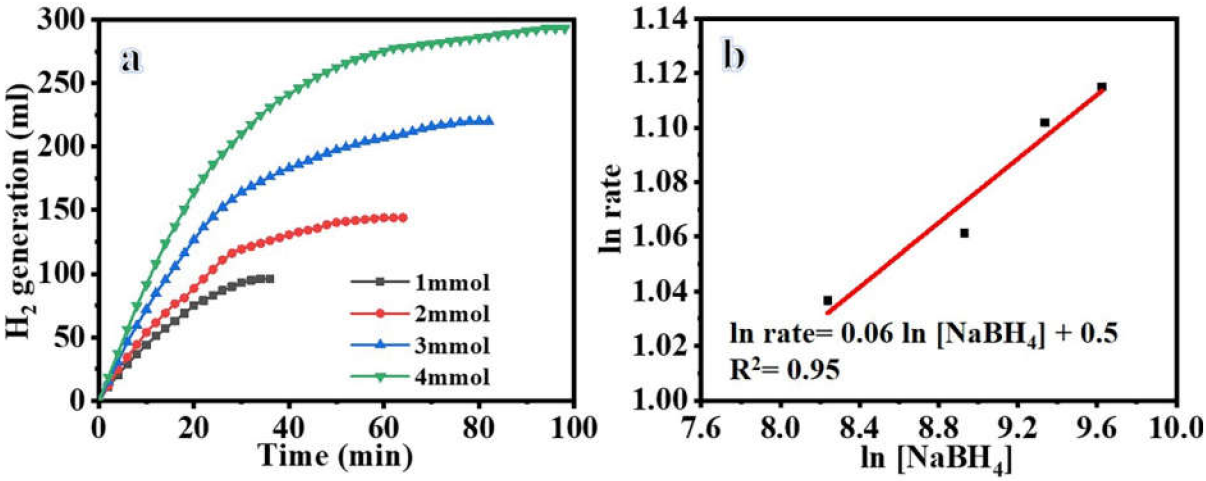


**Figure 8.** The effect of SBH concentration on $H_2$ production (**a**), and the $H_2$ production rate logarithmic value vs. [SBH] concentration logarithmic value (**b**) at 100 mg catalyst and 298 K.

The catalytic performance of the $Ni_{0.3}Cu_{0.7}$/PVDF-HFP catalyst may be affected by the reaction temperature, which in turn affects the chemical kinetic characteristic of the $H_2$ release process. To further understand this, 100 mg of $Ni_{0.3}Cu_{0.7}$/PVDF-HFP catalyst and 1 mmol of SBH were used to conduct experiments at four different reaction temperatures (298 K, 303 K, 308 K, and 328 K). Figure 9a shows that when the reaction temperature is raised, the reaction time for $H_2$ generation decreases. The values of the rate constant, k, can be determined by examining the slope of the linear portion of the plots at various reaction temperatures. Figure 9b displays the ln k vs. 1/T plot that was constructed using the activation parameters for the hydrolysis processes of SBH utilizing $Ni_{0.3}Cu_{0.7}$/PVDF-HFP catalyst, which were determined using the well-known Arrhenius and Eyring equations. For the $Ni_{0.3}Cu_{0.7}$/PVDF-HFP catalyst system, the activation energy for the hydrolysis process of SBH solution was determined to be Ea = 27.81 kJ/mol. The activation energy of the non-noble metal catalyst $Ni_{0.3}Cu_{0.7}$/PVDF-HFP is low when compared to that of Ni-based catalysts and Cu-based catalysts as shown in Table 1. It seems that the fabricated $Ni_{0.3}Cu_{0.7}$/PVDF-HFP catalyst achieves excellent catalytic performance in SBH hydrolysis.

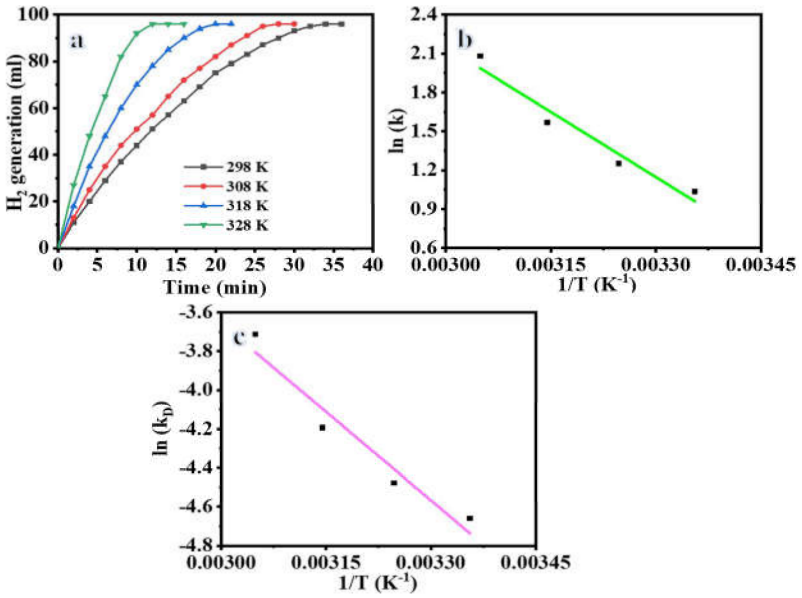


**Figure 9.** Influence of reaction temperature on $H_2$ production (**a**), the $H_2$ production rate constant logarithmic value vs. (1/T) (**b**), and $K_D$ (K/T) logarithmic value vs. (1/T) (**c**) at 100 mg catalyst and 1 mmol [SBH].

**Table 1.** Activation energies of Ni- and Cu-based catalysts for $H_2$ generation from SBH.

| Catalyst | Ea (KJ/mol) | Ref. |
|---|---|---|
| Ni | 42.28 | [70] |
| Ni | 71 | [71] |
| Raney Ni | 63 | [71] |
| Ni-Ag | 16.2 | [72] |
| Ni-Co | 38 | [73] |
| Ni-Co-B | 62 | [74] |
| Co-B/Cu | 43.3 | [75] |
| Co-Cu-Ni | 40.6 | [76] |
| Co-Cu-B/Ni foam | 52 | [77] |
| WSC-Cu | 32.7 | [78] |
| P(EP-g-AA)-Cu | 42.6 | [79] |
| Co-Ni/AC | 68.9 | [19] |
| Co-Ni/MWAC | 40.7 | [80] |
| Sm- Ni-Co-P/g-Al2O3 | 52.1 | [81] |
| Ni–Co–B | 62 | [75] |
| Ni-hollow PVDF capsules | 49.3 | [65] |
| Ni-PVDF hollow fiber | 55.3 | [82] |
| ([C6(mpy)2][NiCl4]2- | 56.4 | [83] |
| PVDF-[C6(mpy)2][NiCl4]2- | 44.6 | [41] |
| NiCu/PVDF-HFP | 27.8 | This study |

To evaluate the catalytic reusability, the same catalyst (100 mg of $Ni_{0.3}Cu_{0.7}$/PVDF-HFP) was utilized up to five times in the reduction processes of 1 mmol SBH at 25 °C with a mixing rate of 1000 rpm (Figure 10). The percentage of conversion remained the same as indicated in Figure 10, but the activity of the catalysts decreased to 93% after four cycles. The remarkable durability should be ascribed to the crystalline structure of the catalyst, which has remained mostly constant, as well as the ultrafine CuNi NPs, which have continued to be well-stabilized at PVDF-HFB throughout the catalytic cycles. It was important to point out that the SBH was introduced to the reactor without separating the catalytic NFs. At the end of each cycle, the hydrolysis process of SBH will have been finished completely. The decrease in catalytic activity, which began after four runs, may be attributed to the following: (1) an increase in the solution viscosity and (2) the passivation of the NFs' surface, which may be attributed to the accumulation of boron products (such as metaborate) on the reaction solution and polymer surface, which inhibited the metal active sites [12].

Equations (3)–(5) were applied to express SBH hydrolysis kinetics as a function of $Ni_{0.3}Cu_{0.7}$/PVDF-HFP concentration, SBH concentration, and reaction temperatures.

$$r = -d[SBH]dt = k[HFB - 40]^{1.1}\left[SBH^{-0.06}\right] \quad (3)$$

$$k = Ae^{\left(\frac{-E_a}{RT}\right)} \rightarrow \ln k = \ln 12.188 - \frac{3345.9}{8.314T} \quad (4)$$

$$r = -d[SBH]dt = 12.1882e^{(-3345.9/T)}[HFB - 40]^{1.1}\left[SBH^{-0.06}\right] \quad (5)$$

The activation enthalpy (ΔH, (KJ/mol)) and the activation entropy (ΔS, (J/mol.K)) may be used to get the Gibbs free energy of activation (ΔG, (KJ/mol)) using Equations (6) and (7).

$$\ln k_D = \ln \frac{k_B}{h} + \frac{\Delta S}{R} - \frac{\Delta H}{RT} \quad (6)$$

$$\Delta G = \Delta H - T\Delta S \quad (7)$$

where $k_D$ = (k/T), $K_B$ is Boltzmann constant ($1.381 \times 10^{-23}$ J·K$^{-1}$), and h is the Planck constant ($6.626 \times 10^{-34}$ J·s$^{-1}$). According to Equation (7) in Figure 9c, ΔH and ΔS is

estimated to be 33.83 kJ $mol^{-1}$ and 0.074 kJ $mol^{-1}$, respectively. Hence, the ΔG equation can be summarized as follows: $\Delta G = 33.83 - 0.074T$.

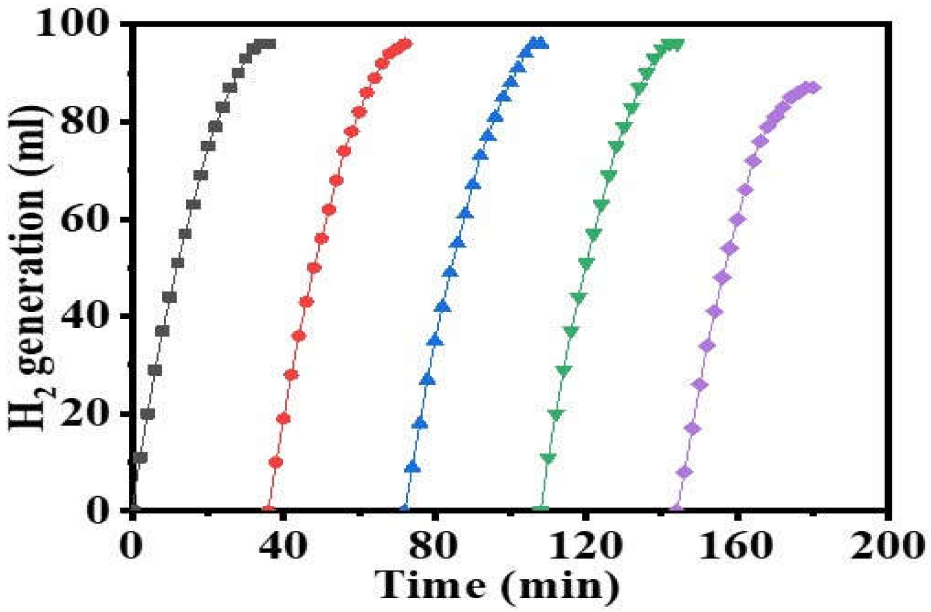


**Figure 10.** Reusability test of $Ni_{0.7}Cu_{0.3}$@PVDF-HFP NF membranes. (The amount of catalyst = 100 mg, (SBH) = 1 mmol, and T = 298 K.)

## 4. Conclusions

CuNi nanoparticles supported on PVDF-HFP nanofibers catalysts have been effectively fabricated by the electrospinning technique and in situ reduction in metal ions. The fabricated bimetal catalysts have presented a superior catalytic performance in $H_2$ generation from SBH as compared to monometallic counterparts. The alloy composed of $Ni_{0.3}Cu_{0.7}$/PVDF-HFP NFs has shown good catalytic activity as compared to other formulations. The excellent catalytic activity is in regard to the synergistic effects between Ni and Cu resulting from their geometric effects and uniform distribution of bimetallic NPs. According to the findings of the kinetics investigations, the reaction follows a zero-order and a first-order mechanism with regard to the SBH concentration and the catalyst amount, respectively. In addition, a low activation energy, evaluated as Ea = 27.81 kJ/mol, was obtained for the hydrolysis process that was performed on the SBH solution.

The catalyst has been reused for five cycles. The great catalytic performance and simple separation of the introduced catalytic NFs make them a promising candidate to be a highly efficient catalyst for a hydrogen storage system that enhances commercial applications.

**Funding:** The author extends his appreciation to the Deputyship for Research & Innovation, Ministry of Education in Saudi Arabia for funding this research work through the project number ISP22-31.

**Institutional Review Board Statement:** Not applicable.

**Informed Consent Statement:** Not applicable.

**Data Availability Statement:** Not applicable.

**Conflicts of Interest:** The author declares no conflict of interest.

## References

1. Guimarães, L.N.D.M.R. Future Energy and the Use of Renewables. In *Affordable and Clean Energy*; Springer: Cham, Switzerland, 2021; Volume 6330, pp. 678–688.
2. Kim, G.J.; Hwang, H.T. Thermal hydrolysis of solid-state sodium borohydride for noncatalytic hydrogen generation. *Chem. Eng. J.* **2021**, *424*, 130445. [CrossRef]

3. Demirci, S.; Suner, S.S.; Yildiz, M.; Sahiner, N. Polymeric ionic liquid forms of PEI microgels as catalysts for hydrogen production via sodium borohydride methanolysis. *J. Mol. Liq.* **2022**, *360*, 119562. [CrossRef]
4. Dutta, S. A review on production, storage of hydrogen and its utilization as an energy resource. *J. Ind. Eng. Chem.* **2014**, *20*, 1148–1156. [CrossRef]
5. Zheng, J.; Wang, C.-G.; Zhou, H.; Ye, E.; Xu, J.; Li, Z.; Loh, X.J. Current research trends and perspectives on solid-state nanomaterials in hydrogen storage. *Research* **2021**, *2021*, 3750689. [CrossRef] [PubMed]
6. Van Hoecke, L.; Laffineur, L.; Campe, R.; Perreault, P.; Verbruggen, S.W.; Lenaerts, S. Challenges in the use of hydrogen for maritime applications. *Energy Environ. Sci.* **2021**, *14*, 815–843. [CrossRef]
7. Yousef, A.; Barakat, N.A.; El-Newehy, M.H.; Ahmed, M.; Kim, H.Y. Catalytic hydrolysis of ammonia borane for hydrogen generation using Cu (0) nanoparticles supported on $TiO_2$ nanofibers. *Colloids Surf. A Physicochem. Eng. Asp.* **2015**, *470*, 194–201. [CrossRef]
8. Yousef, A.; Barakat, N.A.; Khalil, K.A.; Unnithan, A.R.; Panthi, G.; Pant, B.; Kim, H.Y. Photocatalytic release of hydrogen from ammonia borane-complex using Ni (0)-doped $TiO_2$/C electrospun nanofibers. *Colloids Surf. A Physicochem. Eng. Asp.* **2012**, *410*, 59–65. [CrossRef]
9. Yousef, A.; Barakat, N.A.; Kim, H.Y. Electrospun Cu-doped titania nanofibers for photocatalytic hydrolysis of ammonia borane. *Appl. Catal. A Gen.* **2013**, *467*, 98–106. [CrossRef]
10. Bell, C. Hydrogen Fuel Cell Cold Operation. Master's Thesis, University of Minnesota, Minneapolis, MN, USA, 2019.
11. Bogdanović, B.; Felderhoff, M.; Streukens, G. Hydrogen storage in complex metal hydrides. *J. Serb. Chem. Soc.* **2009**, *74*, 183–196. [CrossRef]
12. Abe, J.O.; Popoola, A.P.I.; Ajenifuja, E.; Popoola, O.M. Hydrogen energy, economy and storage: Review and recommendation. *Int. J. Hydrogen Energy* **2019**, *44*, 15072–15086. [CrossRef]
13. Yao, Q.; Ding, Y.; Lu, Z.-H. Noble-metal-free nanocatalysts for hydrogen generation from boron-and nitrogen-based hydrides. *Inorg. Chem. Front.* **2020**, *7*, 3837–3874. [CrossRef]
14. Patel, N.; Miotello, A. Progress in Co–B related catalyst for hydrogen production by hydrolysis of boron-hydrides: A review and the perspectives to substitute noble metals. *Int. J. Hydrogen Energy* **2015**, *40*, 1429–1464. [CrossRef]
15. Al-Enizi, A.M.; Nafady, A.; El-Halwany, M.; Brooks, R.M.; Abutaleb, A.; Yousef, A. Electrospun carbon nanofiber-encapsulated NiS nanoparticles as an efficient catalyst for hydrogen production from hydrolysis of sodium borohydride. *Int. J. Hydrogen Energy* **2019**, *44*, 21716–21725. [CrossRef]
16. Ding, X.-L.; Yuan, X.; Jia, C.; Ma, Z.-F. Hydrogen generation from catalytic hydrolysis of sodium borohydride solution using cobalt–copper–boride (Co–Cu–B) catalysts. *Int. J. Hydrogen Energy* **2010**, *35*, 11077–11084. [CrossRef]
17. Deonikar, V.G.; Rathod, P.V.; Pornea, A.M.; Puguan, J.M.C.; Park, K.; Kim, H. Hydrogen generation from catalytic hydrolysis of sodium borohydride by a Cu and Mo promoted Co catalyst. *J. Ind. Eng. Chem.* **2020**, *86*, 167–177. [CrossRef]
18. Huang, C.-C.; Lo, S.-L.; Lien, H.-L. Zero-valent copper nanoparticles for effective dechlorination of dichloromethane using sodium borohydride as a reductant. *Chem. Eng. J.* **2012**, *203*, 95–100. [CrossRef]
19. Didehban, A.; Zabihi, M.; Shahrouzi, J.R. Experimental studies on the catalytic behavior of alloy and core-shell supported Co-Ni bimetallic nano-catalysts for hydrogen generation by hydrolysis of sodium borohydride. *Int. J. Hydrogen Energy* **2018**, *43*, 20645–20660. [CrossRef]
20. Al-Enizi, A.M.; Brooks, R.M.; Abutaleb, A.; El-Halwany, M.; El-Newehy, M.H.; Yousef, A. Electrospun carbon nanofibers containing Co-TiC nanoparticles-like superficial protrusions as a catalyst for H2 gas production from ammonia borane complex. *Ceram. Int.* **2017**, *43*, 15735–15742. [CrossRef]
21. Al-Enizi, A.M.; Brooks, R.M.; Ahmad, M.; El-Halwany, M.; El-Newehy, M.H.; Yousef, A. In-situ synthesis of amorphous co nanoparticles supported onto $TiO_2$ nanofibers as a catalyst for hydrogen generation from the hydrolysis of ammonia borane. *J. Nanosci. Nanotechnol.* **2018**, *18*, 4714–4719. [CrossRef]
22. Brooks, R.M.; Maafa, I.M.; Al-Enizi, A.M.; El-Halwany, M.M.; Ubaidullah, M.; Yousef, A. Electrospun bimetallic nicr nanoparticles@ carbon nanofibers as an efficient catalyst for hydrogen generation from ammonia borane. *Nanomaterials* **2019**, *9*, 1082. [CrossRef]
23. Saka, C.; Eygi, M.S.; Balbay, A. CoB doped acid modified zeolite catalyst for enhanced hydrogen release from sodium borohydride hydrolysis. *Int. J. Hydrogen Energy* **2020**, *45*, 15086–15099. [CrossRef]
24. Akti, F. Hydrogen generation from hydrolysis of sodium borohydride by silica xerogel supported cobalt catalysts: Positive roles of amine modification and calcination treatment. *Fuel* **2021**, *303*, 121326. [CrossRef]
25. Diban, N.; Pacuła, A.; Kumakiri, I.; Barquín, C.; Rivero, M.J.; Urtiaga, A.; Ortiz, I. $TiO_2$–Zeolite Metal Composites for Photocatalytic Degradation of Organic Pollutants in Water. *Catalysts* **2021**, *11*, 1367. [CrossRef]
26. Daneshyar, A.; Ghaedi, M.; Sabzehmeidani, M.M. $H_2S$ adsorption onto Cu-Zn–Ni nanoparticles loaded activated carbon and Ni-Co nanoparticles loaded $\gamma$-$Al_2O_3$: Optimization and adsorption isotherms. *J. Colloid Interface Sci.* **2017**, *490*, 553–561. [CrossRef] [PubMed]
27. Yousef, A.; Barakat, N.A.; El-Newehy, M.; Kim, H.Y. Chemically stable electrospun NiCu nanorods@ carbon nanofibers for highly efficient dehydrogenation of ammonia borane. *Int. J. Hydrogen Energy* **2012**, *37*, 17715–17723. [CrossRef]
28. Zhang, J.; Li, H.; Zhang, H.; Zhu, Y.; Mi, G. Porously hierarchical Cu@ Ni cubic-cage microstructure: Very active and durable catalyst for hydrolytically liberating $H_2$ gas from ammonia borane. *Renew. Energy* **2016**, *99*, 1038–1045. [CrossRef]

29. Patel, N.; Patton, B.; Zanchetta, C.; Fernandes, R.; Guella, G.; Kale, A.; Miotello, A. Pd-C powder and thin film catalysts for hydrogen production by hydrolysis of sodium borohydride. *Int. J. Hydrogen Energy* **2008**, *33*, 287–292. [CrossRef]
30. Panthi, G.; Barakat, N.A.; Khalil, K.A.; Yousef, A.; Jeon, K.-S.; Kim, H.Y. Encapsulation of CoS nanoparticles in PAN electrospun nanofibers: Effective and reusable catalyst for ammonia borane hydrolysis and dyes photodegradation. *Ceram. Int.* **2013**, *39*, 1469–1476. [CrossRef]
31. Panthi, G.; Barakat, N.A.; Risal, P.; Yousef, A.; Pant, B.; Unnithan, A.R.; Kim, H.Y. Preparation and characterization of nylon-6/gelatin composite nanofibers via electrospinning for biomedical applications. *Fibers Polym.* **2013**, *14*, 718–723. [CrossRef]
32. Yousef, A.; Barakat, N.A.; Amna, T.; Unnithan, A.R.; Al-Deyab, S.S.; Kim, H.Y. Influence of CdO-doping on the photoluminescence properties of ZnO nanofibers: Effective visible light photocatalyst for waste water treatment. *J. Lumin.* **2012**, *132*, 1668–1677. [CrossRef]
33. Afeesh, R.; Barakat, N.A.; Al-Deyab, S.S.; Yousef, A.; Kim, H.Y. Nematic shaped cadmium sulfide doped electrospun nanofiber mat: Highly efficient, reusable, solar light photocatalyst. *Colloids Surf. A Physicochem. Eng. Asp.* **2012**, *409*, 21–29. [CrossRef]
34. Remanan, S.; Padmavathy, N.; Rabiya, R.; Ghosh, S.; Das, T.K.; Bose, S.; Sen, R.; Das, N.C. Converting polymer trash into treasure: An approach to prepare $MoS_2$ nanosheets decorated PVDF sponge for oil/water separation and antibacterial applications. *Ind. Eng. Chem. Res.* **2020**, *59*, 20141–20154. [CrossRef]
35. Das, T.K.; Remanan, S.; Ghosh, S.; Das, N.C. An environment friendly free-standing cellulose membrane derived for catalytic reduction of 4-nitrophenol: A sustainable approach. *J. Environ. Chem. Eng.* **2021**, *9*, 104596. [CrossRef]
36. Chen, C.; Tang, Y.; Vlahovic, B.; Yan, F. Electrospun polymer nanofibers decorated with noble metal nanoparticles for chemical sensing. *Nanoscale Res. Lett.* **2017**, *12*, 451. [CrossRef]
37. Jin, W.J.; Lee, H.K.; Jeong, E.H.; Park, W.H.; Youk, J.H. Preparation of polymer nanofibers containing silver nanoparticles by using poly (N-vinylpyrrolidone). *Macromol. Rapid Commun.* **2005**, *26*, 1903–1907. [CrossRef]
38. Mallick, K.; Witcomb, M.J.; Dinsmore, A.; Scurrell, M.S. Fabrication of a metal nanoparticles and polymer nanofibers composite material by an in situ chemical synthetic route. *Langmuir* **2005**, *21*, 7964–7967. [CrossRef]
39. Yousef, A.; Brooks, R.M.; El-Halwany, M.; Obaid, M.; El-Newehy, M.H.; Al-Deyab, S.S.; Barakat, N.A. A novel and chemical stable Co–B nanoflakes-like structure supported over titanium dioxide nanofibers used as catalyst for hydrogen generation from ammonia borane complex. *Int. J. Hydrogen Energy* **2016**, *41*, 285–293. [CrossRef]
40. Chinnappan, A.; Kang, H.-C.; Kim, H. Preparation of PVDF nanofiber composites for hydrogen generation from sodium borohydride. *Energy* **2011**, *36*, 755–759. [CrossRef]
41. Chinnappan, A.; Kim, H. Nanocatalyst: Electrospun nanofibers of PVDF–Dicationic tetrachloronickelate (II) anion and their effect on hydrogen generation from the hydrolysis of sodium borohydride. *Int. J. Hydrogen Energy* **2012**, *37*, 18851–18859. [CrossRef]
42. Chen, Y.; Liu, L.; Wang, Y.; Kim, H. Preparation of porous PVDF-NiB capsules as catalytic adsorbents for hydrogen generation from sodium borohydride. *Fuel Process. Technol.* **2011**, *92*, 1368–1373. [CrossRef]
43. Li, Q.; Chen, Y.; Lee, D.J.; Li, F.; Kim, H. Preparation of Y-zeolite/$CoCl_2$ doped PVDF composite nanofiber and its application in hydrogen production. *Energy* **2012**, *38*, 144–150. [CrossRef]
44. Kang, H.-C.; Chen, Y.; Arthur, E.E.; Kim, H. Microstructural control of catalyst-loaded PVDF microcapsule membrane for hydrogen generation by NaBH4 hydrolysis. *Int. J. Hydrogen Energy* **2014**, *39*, 15656–15664. [CrossRef]
45. Li, F.; Arthur, E.E.; La, D.; Li, Q.; Kim, H. Immobilization of $CoCl_2$ (cobalt chloride) on PAN (polyacrylonitrile) composite nanofiber mesh filled with carbon nanotubes for hydrogen production from hydrolysis of NaBH4 (sodium borohydride). *Energy* **2014**, *71*, 32–39. [CrossRef]
46. Abbas, M.; Hameed, R.A.; Al-Enizi, A.M.; Thamer, B.M.; Yousef, A.; El-Newehy, M.H. Decorated carbon nanofibers with mixed nickel− manganese carbides for methanol electro-oxidation in alkaline solution. *Int. J. Hydrogen Energy* **2021**, *46*, 6494–6512. [CrossRef]
47. Abutaleb, A.; Zouli, N.; El-Halwany, M.; Ubaidullah, M.; Yousef, A. Graphitic nanofibers supported NiMn bimetallic nanoalloys as catalysts for H2 generation from ammonia borane. *Int. J. Hydrogen Energy* **2021**, *46*, 35248–35260. [CrossRef]
48. Al-Enizi, A.M.; Brooks, R.M.; El-Halwany, M.; Yousef, A.; Nafady, A.; Hameed, R.A. CoCr7C3-like nanorods embedded on carbon nanofibers as effective electrocatalyst for methanol electro-oxidation. *Int. J. Hydrogen Energy* **2018**, *43*, 9943–9953. [CrossRef]
49. Al-Enizi, A.M.; El-Halwany, M.; Al-Abdrabalnabi, M.A.; Bakrey, M.; Ubaidullah, M.; Yousef, A. Novel Low Temperature Route to Produce CdS/ZnO Composite Nanofibers as Effective Photocatalysts. *Catalysts* **2020**, *10*, 417. [CrossRef]
50. Alkaykh, S.; Mbarek, A.; Ali-Shattle, E.E. Photocatalytic degradation of methylene blue dye in aqueous solution by $MnTiO_3$ nanoparticles under sunlight irradiation. *Heliyon* **2020**, *6*, e03663. [CrossRef]
51. Amna, T.; Hassan, M.S.; Yousef, A.; Mishra, A.; Barakat, N.A.; Khil, M.-S.; Kim, H. Inactivation of foodborne pathogens by NiO/$TiO_2$ composite nanofibers: A novel biomaterial system. *Food Bioprocess Technol.* **2013**, *6*, 988–996. [CrossRef]
52. Babu, K.J.; Senthilkumar, N.; Kim, A.R. Freestanding and binder free PVdF-HFP/Ni-Co nanofiber membrane as a versatile platform for the electrocatalytic oxidation and non-enzymatic detection of urea. *Sens. Actuators B Chem.* **2017**, *241*, 541–551. [CrossRef]
53. Kumar, A.; Logapperumal, S.; Sharma, R.; Das, M.K.; Kar, K.K. Li-ion transport, structural and thermal studies on lithium triflate and barium titanate incorporated poly (vinylidene fluoride-co-hexafluoropropene) based polymer electrolyte. *Solid State Ion.* **2016**, *289*, 150–158. [CrossRef]

54. Elwan, H.A.; Mamlouk, M.; Scott, K. A review of proton exchange membranes based on protic ionic liquid/polymer blends for polymer electrolyte membrane fuel cells. *J. Power Sources* **2021**, *484*, 229197. [CrossRef]
55. Nunes-Pereira, J.; Kundu, M.; Gören, A.; Silva, M.M.; Costa, C.M.; Liu, L.; Lanceros-Méndez, S. Optimization of filler type within poly (vinylidene fluoride-co-trifluoroethylene) composite separator membranes for improved lithium-ion battery performance. *Compos. Part B Eng.* **2016**, *96*, 94–102. [CrossRef]
56. Tian, X.; Jiang, X. Poly (vinylidene fluoride-co-hexafluoropropene)(PVDF-HFP) membranes for ethyl acetate removal from water. *J. Hazard. Mater.* **2008**, *153*, 128–135. [CrossRef]
57. Al-Enizi, A.M.; Yousef, A.; Shaikh, S.F.; Pandit, B.; El-Halwany, M.M. Electrospun Nickel Nanoparticles@ Poly (vinylidene fluoride-hexafluoropropylene) Nanofibers as Effective and Reusable Catalyst for $H_2$ Generation from Sodium Borohydride. *Arab. J. Chem.* **2022**, *15*, 104207. [CrossRef]
58. Aydın, K.; Kulaklı, B.N.; Coşkuner Filiz, B.; Alligier, D.; Demirci, U.B.; Kantürk Figen, A. Closing the hydrogen cycle with the couple sodium borohydride-methanol, via the formation of sodium tetramethoxyborate and sodium metaborate. *Int. J. Energy Res.* **2020**, *44*, 11405–11416. [CrossRef]
59. Lo, C.-t.F.; Karan, K.; Davis, B.R. Kinetic studies of reaction between sodium borohydride and methanol, water, and their mixtures. *Ind. Eng. Chem. Res.* **2007**, *46*, 5478–5484. [CrossRef]
60. Zhang, H.; Xu, G.; Zhang, L.; Wang, W.; Miao, W.; Chen, K.; Cheng, L.; Li, Y.; Han, S. Ultrafine cobalt nanoparticles supported on carbon nanospheres for hydrolysis of sodium borohydride. *J. Renew. Energy* **2020**, *162*, 345–354. [CrossRef]
61. Gibson, P.; Schreuder-Gibson, H.; Rivin, D. Transport properties of porous membranes based on electrospun nanofibers. *Colloids Surf. A Physicochem. Eng. Asp.* **2001**, *187*, 469–481. [CrossRef]
62. Yousef, A.; Barakat, N.A.; Al-Deyab, S.S.; Nirmala, R.; Pant, B.; Kim, H.Y. Encapsulation of CdO/ZnO NPs in PU electrospun nanofibers as novel strategy for effective immobilization of the photocatalysts. *Colloids Surf. A Physicochem. Eng. Asp.* **2012**, *401*, 8–16. [CrossRef]
63. Shin, J.; Nho, Y.-C.; Hwang, I.S.; Fei, G.; Kim, A.R.; Nahm, K.S. Irradiated PVdF-HFP–tin oxide composite membranes for the applications of direct methanol fuel cells. *J. Membr. Sci.* **2010**, *350*, 92–100.
64. Kumar, G.G. Irradiated PVdF-HFP-montmorillonite composite membranes for the application of direct ethanol fuel cells. *J. Mater. Chem.* **2011**, *21*, 17382–17391. [CrossRef]
65. Chen, Y.; Shi, Y.; Wang, Y. Preparation of hollow poly (vinylidene fluoride) capsules containing nickel catalyst for hydrogen storage and production. *Int. J. Energy Res.* **2015**, *39*, 634–642. [CrossRef]
66. Babu, K.J.; Yoo, D.J.; Kim, A.R. Binder free and free-standing electrospun membrane architecture for sensitive and selective non-enzymatic glucose sensors. *RSC Adv.* **2015**, *5*, 41457–41467.
67. Kumar, G.G.; Nahm, K.S.; Elizabeth, R.N. Electro chemical properties of porous PVdF-HFP membranes prepared with different nonsolvents. *J. Membr. Sci.* **2008**, *325*, 117–124. [CrossRef]
68. Mandal, B.P.; Vasundhara, K.; Abdelhamid, E.; Lawes, G.; Salunke, H.G.; Tyagi, A.K. Improvement of magnetodielectric coupling by surface functionalization of nickel nanoparticles in Ni and polyvinylidene fluoride nanohybrids. *J. Phys. Chem. C* **2014**, *118*, 20819–20825. [CrossRef]
69. Nath, A.; Kumar, A. Swift heavy ion irradiation induced enhancement in electrochemical properties of ionic liquid based PVdF-HFP-layered silicate nanocomposite electrolyte membranes. *J. Membr. Sci.* **2014**, *453*, 192–201. [CrossRef]
70. Ozay, O.; Aktas, N.; Inger, E.; Sahiner, N. Hydrogel assisted nickel nanoparticle synthesis and their use in hydrogen production from sodium boron hydride. *Int. J. Hydrogen Energy* **2011**, *36*, 1998–2006. [CrossRef]
71. Kaufman, C.M.; Sen, B. Hydrogen generation by hydrolysis of sodium tetrahydroborate: Effects of acids and transition metals and their salts. *J. Chem. Soc. Dalton Trans.* **1985**, 307–313. [CrossRef]
72. Al-Thabaiti, S.A.; Khan, Z.; Malik, M.A. Bimetallic Ag-Ni nanoparticles as an effective catalyst for hydrogen generation from hydrolysis of sodium borohydride. *Int. J. Hydrogen Energy* **2019**, *44*, 16452–16466. [CrossRef]
73. Kim, J.-H.; Lee, H.; Han, S.-C.; Kim, H.-S.; Song, M.-S.; Lee, J.-Y. Production of hydrogen from sodium borohydride in alkaline solution: Development of catalyst with high performance. *Int. J. Hydrogen Energy* **2004**, *29*, 263–267. [CrossRef]
74. Ingersoll, J.C.; Mani, N.; Thenmozhiyal, J.C.; Muthaiah, A. Catalytic hydrolysis of sodium borohydride by a novel nickel–cobalt–boride catalyst. *J. Power Sources* **2007**, *173*, 450–457. [CrossRef]
75. Wang, Y.; Li, T.; Bai, S.; Qi, K.; Cao, Z.; Zhang, K.; Wu, S.; Wang, D. Catalytic hydrolysis of sodium borohydride via nanostructured cobalt–boron catalysts. *Int. J. Hydrogen Energy* **2016**, *41*, 276–284. [CrossRef]
76. Wang, X.; Zhao, Y.; Peng, X.; Jing, C.; Hu, W.; Tian, S.; Tian, J. In situ synthesis of cobalt-based tri-metallic nanosheets as highly efficient catalysts for sodium borohydride hydrolysis. *Int. J. Hydrogen Energy* **2016**, *41*, 219–226. [CrossRef]
77. Wang, Y.; Zou, K.; Zhang, D.; Cao, Z.; Zhang, K.; Xie, Y.; Li, G.; Bai, S. Cobalt–copper–boron nanoparticles as catalysts for the efficient hydrolysis of alkaline sodium borohydride solution. *Int. J. Hydrogen Energy* **2020**, *45*, 9845–9853. [CrossRef]
78. Ding, J.; Li, Q.; Su, Y.; Yue, Q.; Gao, B.; Zhou, W. Preparation and catalytic activity of wheat straw cellulose based hydrogel-nanometal composites for hydrogen generation from NaBH4 hydrolysis. *Int. J. Hydrogen Energy* **2018**, *43*, 9978–9987. [CrossRef]
79. Zhao, L.; Li, Q.; Su, Y.; Yue, Q.; Gao, B. A novel Enteromorpha based hydrogel for copper and nickel nanoparticle preparation and their use in hydrogen production as catalysts. *Int. J. Hydrogen Energy* **2017**, *42*, 6746–6756. [CrossRef]
80. Soltani, M.; Zabihi, M. Hydrogen generation by catalytic hydrolysis of sodium borohydride using the nano-bimetallic catalysts supported on the core-shell magnetic nanocomposite of activated carbon. *Int. J. Hydrogen Energy* **2020**, *45*, 12331–12346. [CrossRef]

81. Li, Z.; Li, H.; Wang, L.; Liu, T.; Zhang, T.; Wang, G.; Xie, G. Hydrogen generation from catalytic hydrolysis of sodium borohydride solution using supported amorphous alloy catalysts (Ni–Co–P/γ-$Al_2O_3$). *Int. J. Hydrogen Energy* **2014**, *39*, 14935–14941. [CrossRef]
82. Chen, Y.; Shi, Y.; Liu, X.; Zhang, Y. Preparation of polyvinylidene fluoride–nickel hollow fiber catalytic membranes for hydrogen generation from sodium borohydride. *Fuel* **2015**, *140*, 685–692. [CrossRef]
83. Chinnappan, A.; Kim, H.; Baskar, C.; Hwang, I.T. Hydrogen generation from the hydrolysis of sodium borohydride with new pyridinium dicationic salts containing transition metal complexes. *Int. J. Hydrogen Energy* **2012**, *37*, 10240–10248. [CrossRef]

**Disclaimer/Publisher's Note:** The statements, opinions and data contained in all publications are solely those of the individual author(s) and contributor(s) and not of MDPI and/or the editor(s). MDPI and/or the editor(s) disclaim responsibility for any injury to people or property resulting from any ideas, methods, instructions or products referred to in the content.